

The ESO UVES Advanced Data Products Quasar Sample - I. Dataset and New N_{HI} Measurements of Damped Absorbers

Tayyaba Zafar¹, Attila Popping², and Céline Péroux¹

¹ Aix Marseille Université, CNRS, LAM (Laboratoire d’Astrophysique de Marseille) UMR 7326, 13388, Marseille, France.

² International Centre for Radio Astronomy Research (ICRAR), The University of Western Australia, 35 Stirling Hwy, Crawley, WA 6009, Australia.

Received / Accepted

ABSTRACT

We present here a dataset of quasars observed with the Ultraviolet Visual Echelle Spectrograph (UVES) on the Very Large Telescope and available in the European Southern Observatory UVES Advanced Data Products archive. The sample is made up of a total of 250 high resolution quasar spectra with emission redshifts ranging from $0.191 \leq z_{\text{em}} \leq 6.311$. The total UVES exposure time of this dataset is 1560 hours. Thanks to the high resolution of UVES spectra, it is possible to unambiguously measure the column density of absorbers with damping wings, down to $N_{HI} \gtrsim 10^{19} \text{ cm}^{-2}$, which constitutes the sub-damped Ly α absorber (sub-DLA) threshold. Within the wavelength coverage of our UVES data, we find 150 damped Ly α systems (DLAs)/sub-DLAs in the range $1.5 < z_{\text{abs}} < 4.7$. Of these 150, 93 are DLAs and 57 are sub-DLAs. An extensive search in the literature indicates that 6 of these DLAs and 13 of these sub-DLAs have their N_{HI} measured for the first time. Among them, 10 are new identifications as DLAs/sub-DLAs. For each of these systems, we obtain an accurate measurement of the H i column density and the absorber’s redshift in the range $1.7 < z_{\text{abs}} < 4.2$ by implementing a Voigt profile-fitting algorithm. These absorbers are further confirmed thanks to the detection of associated metal lines and/or lines from members of the Lyman series. In our data, a few quasars’ lines-of-sight are rich. An interesting example is towards QSO J0133+0400 ($z_{\text{em}} = 4.154$) with six DLAs and sub-DLAs reported.

Key words. Galaxies: abundances – Galaxies: high-redshift – Quasars: absorption lines – Quasars: general.

1. Introduction

Among the absorption systems observed in the spectra of quasars, those with the highest neutral hydrogen column density are thought to be connected with the gas reservoir responsible for forming galaxies at high redshift and have deserved wide attention (see review by Wolfe et al. 2005). These systems are usually classified according to their neutral hydrogen column density as damped Ly α systems (hereafter DLAs) with $N_{HI} \geq 2 \times 10^{20}$ atoms cm^{-2} (e.g., Storrie-Lombardi & Wolfe 2000; Wolfe et al. 2005) and sub-damped Ly α systems (sub-DLAs) with $10^{19} \leq N_{HI} \leq 2 \times 10^{20}$ atoms cm^{-2} (e.g., Péroux et al. 2003a).

The study of these systems has made significant progress in recent years, thanks to the availability of large sets of quasar spectra with the two-degree field survey (2dF, Croom et al. 2001) and the Sloan Digital Sky Survey (SDSS; Prochaska et al. 2005; Noterdaeme et al. 2009; Noterdaeme et al. 2012b). They have been shown to contain most of the neutral gas mass in the Universe (Lanzetta et al. 1991, 1995; Wolfe et al. 1995) and are currently used to measure the redshift evolution of the total amount of neutral gas mass density (Lanzetta et al. 1991; Wolfe et al. 1995; Storrie-Lombardi & Wolfe 2000; Péroux et al. 2003b; Prochaska et al. 2005; Noterdaeme et al. 2009, 2012b). In addition, the sub-DLAs may contribute significantly to the cosmic metal budget, which is still highly incomplete. Indeed, only $\sim 20\%$ of the metals are observed when one adds the contribution of the Ly α forest, DLAs, and galaxies such as Lyman break galaxies (e.g., Pettini et al. 1999; Pagel

2002; Wolfe et al. 2003; Pettini 2004, 2006; Bouché et al. 2005, 2006, 2007).

Therefore, to obtain a complete picture of the redshift evolution of both the cosmological neutral gas mass density and the metal content of the Universe, the less-studied sub-DLAs should be taken into account (Péroux et al. 2003a). However, these systems cannot be readily studied at low resolution, and only limited samples of high-resolution quasar spectra have been available until now (e.g., Péroux et al. 2003a; Dessauges-Zavadsky et al. 2003; Ledoux et al. 2003; Kulkarni et al. 2007; Meiring et al. 2008, 2009). The excellent resolution and large wavelength coverage of UVES allows this less studied class of absorber to be explored.

We have therefore examined the high-resolution quasar spectra taken between February 2000 and March 2007 and available in the UVES (Dekker et al. 2000) Advanced Data Products archive, ending up with a sample of 250 quasar spectra. In this paper we present both the dataset of quasars observed with UVES and the damped absorbers (DLAs and sub-DLAs) covered by these spectra. In addition, we measured column densities of DLAs/sub-DLAs seen in the spectra of these quasars and not reported in the literature. In a companion paper (Zafar et al. 2013), we built a carefully selected subset of this dataset to study the statistical properties of DLAs and sub-DLAs, their column density distribution, and the contribution of sub-DLAs to the gas mass density. Further studies, based on specifically designed subsets of the dataset built in this paper, will follow (e.g., studies of metal abundances, molecules).

This work is organized as follows. In §2, information about the UVES quasar data sample is provided. In §3, the properties

of the damped absorbers are described. This section also summarizes the details of the new column density measurements. In §4, some global properties of the full sample are presented and lines-of-sight of interest are reported in §5. All log values and expressions correspond to log base 10.

2. The Quasar Sample

2.1. ESO Advanced Data Products

In 2007, the European Southern Observatory (ESO) managing the 8.2m Very Large Telescope (VLT) observatory has made available to the international community a set of Advanced Data Products for some of its instruments, including the high-resolution UVES¹ instrument. The reduced archival UVES echelle dataset is processed by the ESO UVES pipeline (version 3.2) within the MIDAS environment with the best available calibration data. This process has been executed by the quality control (QC) group, part of the Data Flow Department. The resulting sample is based on an uniform reprocessing of UVES echelle point source data from the beginning of operations (dated 18th of February 2000) up to the 31st of March 2007. The standard quality assessment, quality control and certification have been integral parts of the process. The following types of UVES data are not included in the product data set: *i*) data using the image slicers and/or the absorption cell; *ii*) Echelle data from extended objects and *iii*) data from the Fibre Large Array Multi Element Spectrograph (FLAMES)/UVES instrument mode.

In general, no distinction has been made between visitor mode (VM) and service mode (SM) data, nor between standard settings and non-standard settings. However, the data reduction was performed only when robust calibration solutions i.e., (“master calibrations”) were available. In the UVES Advanced Data Products archive, these calibrations are available only for the standard settings centered on λ 346, 390, 437, 520, 564, 580, 600 or 860 nm. For certain “non-standard” settings, master calibrations were not produced in the first years of UVES operations (until about 2003). These are e.g. 1x2 or 2x3 binnings, or the central wavelengths mentioned above. As a result, the Advanced Data Products database used for the study presented here is not as complete as the ESO UVES raw data archive.

2.2. Quasars Selection

The UVES archives do not provide information on the nature of the targets. Indeed, the target names are chosen by the users and only recently does the Phase 2 step propose for the user to classify the targets, but only on a voluntary-basis. Therefore, the first step to construct a sample of quasar spectra out of the Advanced Data Products archive is to identify the nature of the objects. For this purpose we retrieved quasar lists issued from quasar surveys: the Sloan digital sky survey data release 7 (DR7) database², HyperLeda³, 2dF quasar redshift survey⁴, Simbad⁵ and the Hamburg ESO catalogue. The resulting right ascension (RA) and declination (Dec) of the quasars were cross-matched with UVES Advanced Data Products archive within a radius of 15.0''. The large radius was chosen to overcome possible relative astrometric shifts between the various surveys and the UVES

database. Because of this large radius, the raw matched list do not only contain quasars but also other objects such as stars, galaxies, Seyferts. The non-quasar objects have been filtered out by visual inspection of the spectra. The data in an ESO OPC category C (Interstellar Medium, Star Formation and Planetary Systems) and D (Stellar Evolution) are usually targeting galactic objects, but for some cases observers targeted quasars under the same program. The spectra have been visually inspected for those particular cases.

2.3. Further Data Processing

In the UVES spectrograph, the light beam from the telescope is split into two arms (UV to Blue and Visual to Red) within the instrument. The spectral resolution of UVES is about $R = \lambda/\Delta\lambda \sim 41,400$ when a 1.0'' slit is used. By varying slit width, the maximum spectral resolution can reach up to $R = 80,000$ and 110,000 for the BLUE and the RED arm, respectively. For each target, individual spectra (most often with overlapping settings) were merged using a dedicated Python code which weights each spectrum by its signal-to-noise ratio. All contributing spectra were regridded to a common frame, with the resolution being that of the spectrum with the highest sampling. When present, the bad pixels were masked to assure that they would not contribute to the merged spectrum. In the regions of overlap the spectra were calibrated to the same level before being error-weighted and merged. Particular attention was given to “step” features in the quasar continua and a visual search has identified and corrected these features when they corresponded to the position in between two orders of the Echelle spectrum. In the merging process for each individual spectrum, a radial velocity correction for barycentric and heliocentric motion (using heliocentric correction values from the files header) was applied. A vacuum correction on the wavelength was also applied.

The resulting list comprises 250 quasar spectra. The number of individual spectra used to produce the co-added spectrum, Simbad V-band magnitudes, together with total exposure time in seconds for each target, are provided in Table 1. Throughout the paper, this sample obtained from the ESO UVES Advanced Data Products facility is called EUADP sample. The total VLT exposure time of this dataset is $T_{tot} = 1560$ hours.

In the case of close pairs of quasars or gravitationally-lensed quasars, we have separated the objects if different slit-positions were used but only analyzed the brightest object if these objects were aligned along the slit. Our sample contains two lensed quasars: QSO B0908+0603 (double system) and QSO B1104-181 (quadruple system). In the former case two objects, and, in the latter case, three objects were aligned on the slit (Lopez et al. 2007). In these cases we only analyzed the brightest objects. Our sample contains four quasar pairs: QSO J0008-2900 & QSO J0008-2901 (separated by 1.3'), J030640.8-301032 & J030643.7-301107 (separated by ~0.85'), QSO B0307-195A & B (separated by ~1'), and QSO J1039-2719 & QSO B1038-2712 (separated by 17.9'). For these eight objects, eight different slit-positions were used.

3. The DLA/sub-DLA Sample

The quasar spectra were normalized to unity within the MIDAS environment. For each quasar the local continuum was determined in the merged spectrum by using a spline function to smoothly connect the regions free of absorption features (see Fig. 1). The final normalized spectra used for column density

¹ http://archive.eso.org/eso/eso_archive_adp.html

² <http://www.sdss.org/dr7/>

³ <http://leda.univ-lyon1.fr/>

⁴ http://www.2dfquasar.org/Spec_Cat/2qzsearch2.html

⁵ <http://simbad.u-strasbg.fr/>

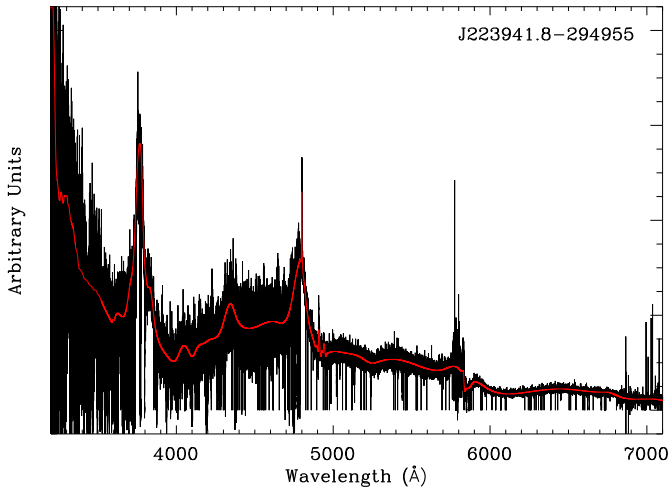


Fig. 1. An example of a UVES quasar spectrum of J223941.8-294955 at $z_{\text{em}} = 2.102$. The quasar continuum (red overlay) is fitted using a spline function.

analysis were obtained by dividing merged spectra by these continua. During normalization, the artifact from residual fringes (especially in standard setting centered on $\lambda 860\text{nm}$) and spectral gaps are also included in the spline fitting. In order to secure all DLAs and sub-DLAs in a given spectrum, we proceeded as in Lanzetta et al. (1991) and used an automated Python detection algorithm. This code builds an equivalent width spectrum over 400 pixel wide boxes ($\sim 12\text{\AA}$ for 0.03\AA pixel $^{-1}$) blueward of the quasar's Ly α emission and flags regions of the spectra where the observed equivalent width exceeds the sub-DLA definition (i.e. $N_{\text{HI}} \gtrsim 10^{19}\text{ cm}^{-2}$). This candidate list of DLAs and sub-DLAs is further supplemented by visual inspection done by TZ and CP. The DLAs and sub-DLAs have been confirmed by looking for associated metal lines and/or higher members of the Lyman series. This resulted in 150 DLAs/sub-DLAs with $1.6 < z_{\text{abs}} < 4.7$ for which Ly α is covered in the spectra of these quasars. This method is complete down to the sub-DLA definition of $N_{\text{HI}} = 10^{19}$ equivalent to $\text{EW}_{\text{rest}} = 2.5\text{\AA}$ based on a curve of growth analysis (Dessauges-Zavadsky et al. 2003).

3.1. N_{HI} measurements of DLAs and sub-DLAs

An extensive search in the literature was undertaken to identify which of these damped absorbers were already known. Of the 150 DLAs/sub-DLAs that we have identified above, 131 (87 DLAs and 44 sub-DLAs) have their N_{HI} already reported in the literature. Of the remaining 19 (6 DLAs and 13 sub-DLAs), 10 (3 DLAs and 7 sub-DLAs) are new identifications (see Table 2 and §3.2 for details on each system).

For damped absorbers, the Lorentzian component of the Voigt profile results in pronounced damping wings, allowing precise determination of N_{HI} down to the sub-DLA definition at high-resolution. The neutral hydrogen column density measurements of these absorbers are determined by fitting a Voigt profile to the Ly α absorption line. The fits were performed using the χ^2 minimization routine FITLYMAN package in MIDAS (Fontana & Ballester 1995). Laboratory wavelengths and oscillator strengths from Morton (2003) were used. The global fit returns the best fit parameters for central wavelength, column density, and Doppler turbulent broadening, as well as errors on each quantity. The central redshift was left as a free parameter

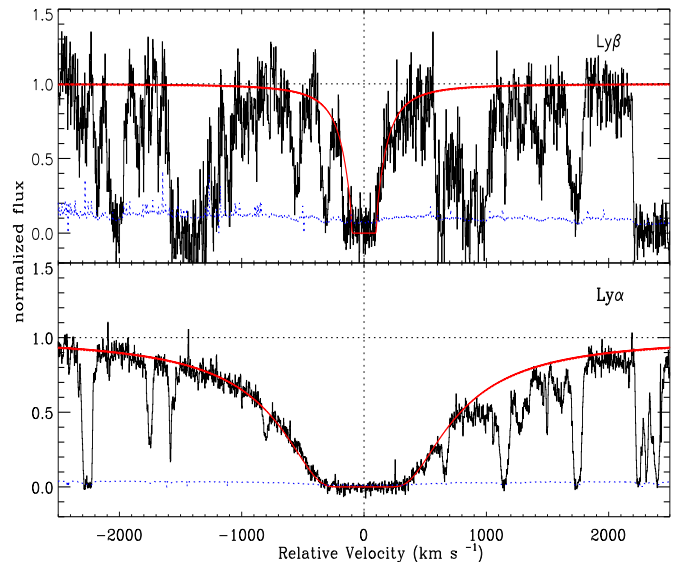


Fig. 2. The sub-DLA detected towards QSO J0008-2900 at $z_{\text{abs}} = 2.254$. The solid red line shows the Voigt profile fit to the sub-DLA with an inferred column density of $\log N_{\text{HI}} = 20.22 \pm 0.10$. The system is detected down to Ly β . Here and in the following figures, the dotted blue line represents 1σ error on the spectrum. The vertical dotted line is the adopted zero velocity corresponding to the redshift of the sub-DLA. The horizontal line is at a level of one.

except when no satisfactory fit could be found in which case the strongest component of the metal line was chosen as central redshift. The Doppler turbulent parameter b -value was usually left as a free parameter and sometimes fixed because of low signal-to-noise or multiple DLAs at 30 km s^{-1} (for DLAs) or 20 km s^{-1} (for sub-DLAs). The N_{HI} fit is performed using the higher members of the Lyman series, in addition to Ly α , where these are available. For fitting N_{HI} , we usually used the components from O I. The other low ionization line components are used to fit N_{HI} for the cases where there is no O I covered by our data. Table 2 summarizes the properties of the DLAs/sub-DLAs for which we obtained HI column density for the first time and provides quasar emission redshifts, absorption redshifts, H I column densities and metal line lists.

Moreover, the majority of the N_{HI} measurements of the DLAs/sub-DLAs towards the 250 EUADP quasars comes from high-resolution data mostly from UVES or Keck/HIRES. In 7 cases, we cover the DLA/sub-DLA in our data but the N_{HI} in the literature is obtained from low/moderate resolution spectra. For these 7 cases, we refitted the DLA/sub-DLA using the EUADP data and new N_{HI} are reported in Table 3. For most of the cases, we find consistent results with the low resolution studies. In the case of QSO B1114-0822, Storrie-Lombardi & Wolfe (2000) reported a DLA with $\log N_{\text{HI}} = 20.3$ at $z_{\text{abs}} = 4.258$ while we find a sub-DLA with $\log N_{\text{HI}} = 20.02 \pm 0.12$.

3.2. Notes on Individual Objects

In this section, we provide details on the DLAs and sub-DLAs in the EUADP sample for which HI column density is determined in this work. Best fit parameters of the Voigt profile fits to the H I absorption lines are detailed below.

1. QSO J0008-2900 ($z_{\text{em}} = 2.645$). The quasar was discovered during the course of the 2dF quasar redshift survey

Table 2. List of 6 damped and 13 sub-damped absorbers with new N_{HI} measurements. The details of these absorbers are provided in the columns as (1) Simbad quasar name, (2) emission redshift, (3) absorption redshift, (4) H α column density with corresponding errors, (5) members of Lyman series covered, (6) metal lines associated with the system, and (7) is the absorber a new identification as DLA/sub-DLA?

Quasar	z_{em}	z_{abs}	$\log N_{\text{HI}}$ cm^{-2}	Ly series	Metals	New?
QSO J0008-2900	2.645	2.254	20.22 ± 0.10	Ly β	O i , Fe ii , Si ii , C ii , Mg ii , Al iii , Si iv	no
QSO J0008-2901	2.607	2.491	19.94 ± 0.11	Ly γ	O i , Fe ii , Si ii , C ii , Al ii , Si iv	no
QSO J0041-4936	3.240	2.248	20.46 ± 0.13	Ly β	O i , Fe ii , Si ii , C ii , Al ii , Zn ii , Al iii , C iv	no
QSO B0128-2150	1.900	1.857	20.21 ± 0.09	Ly α	O i , Fe ii , Si ii , C ii , Al iii	no
J021741.8-370100	2.910	2.429	20.62 ± 0.08	Ly β	O i , Si ii	no
...	...	2.514	20.46 ± 0.09	Ly β	Fe ii , Si ii	no
J060008.1-504036	3.130	2.149	20.40 ± 0.12	Ly α	O i , Fe ii , Si ii , C ii , Al ii , Al iii	yes
QSO B0952-0115	4.426	3.476	20.04 ± 0.07	Ly α	Fe ii , Si ii , Al ii , Al iii , C iv	yes
Q1036-272	3.090	2.792	20.65 ± 0.13	Ly β	O i , Fe ii , Si ii , Al iii	yes
QSO B1036-2257	3.130	2.533	19.30 ± 0.10	Ly α	Fe ii , Si ii , C ii , Al iii , Si iv , C iv	no
QSO B1036-268	2.460	2.235	19.96 ± 0.09	Ly β	O i , Fe ii , Si ii , C ii , Al ii , Mg ii , Al iii , Si iv , C iv	yes
LBQS 1232+0815	2.570	1.720	19.48 ± 0.13	Ly α	O i , Fe ii , Si ii , Al iii , Si iv , C iv	yes
QSO J1330-2522	3.910	2.654	19.56 ± 0.13	Ly α	Si ii , Al ii , Al iii , Si iv , C iv	yes
QSO J1356-1101	3.006	2.397	19.88 ± 0.09	Ly α	O i , Fe ii , Si ii	yes
QSO J1723+2243	4.520	4.155	19.23 ± 0.12	Ly γ	metal lines blended or not covered	yes
LBQS 2114-4347	2.040	1.912	19.50 ± 0.10	Ly α	O i , Fe ii , Si ii , C ii , Al ii , Mg ii , Si iv , C iv	yes
J223941.8-294955	2.102	1.825	19.84 ± 0.14	Ly α	O i , Fe ii , Si ii , C ii , Al ii , Mg ii , Al iii , Si iv , C iv	no
QSO B2318-1107	2.960	1.629	20.52 ± 0.14	Ly α	Fe ii , Si ii , C ii , Al ii , Al iii , Si iv	yes
QSO B2342+3417	3.010	2.940	20.18 ± 0.10	Ly γ	limited red wavelength coverage	no

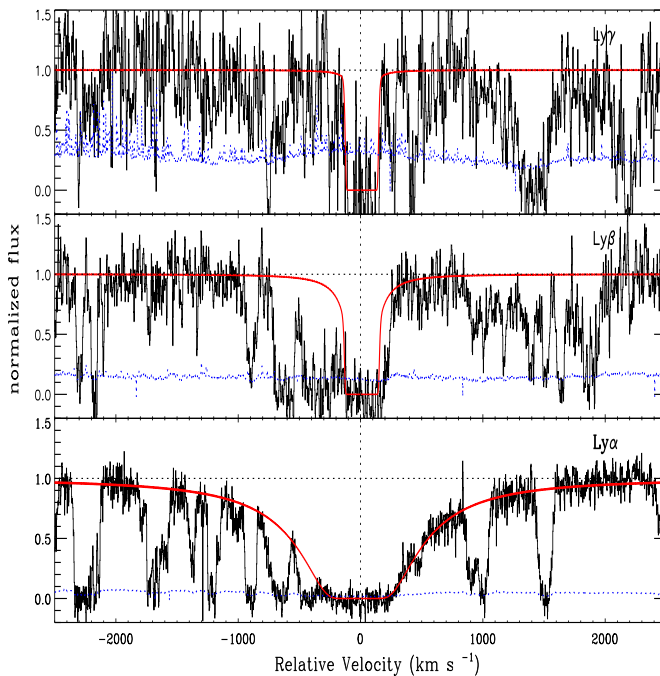


Fig. 3. The sub-DLA detected towards QSO J0008-2901 at $z_{\text{abs}} = 2.491$. The solid red line corresponds to the Voigt profile fit to the sub-DLA with an inferred column density of $\log N_{\text{HI}} = 19.94 \pm 0.11$. The system is detected down to Ly γ .

(Croom et al. 2001). An H α absorber at $z = 2.253$ is reported by Tytler et al. (2009). We find that the absorber is a sub-DLA with $\log N_{\text{HI}} = 20.22 \pm 0.10$ and $b = 28.5 \pm 2.2 \text{ km s}^{-1}$ at $z_{\text{abs}} = 2.254$. The Lyman series lines down to Ly β are fitted together. In the red part of the spectrum metal lines from O i λ 1302, Fe ii $\lambda\lambda\lambda\lambda$ 2344, 2374, 2382, 2586, Si ii $\lambda\lambda\lambda\lambda$ 1260, 1304, 1526, 1808, C ii λ 1334, Al ii λ 1670, and Si iv $\lambda\lambda$ 1393, 1402 are detected in the red part of the spectrum. Fig. 3 shows our best fit result of the H α lines.

Table 3. New high-resolution N_{HI} measurements of DLAs/sub-DLAs previously observed at low/medium resolution.

Quasar	z_{abs}	High resolution $\log N_{\text{HI}}$ cm^{-2}	Low/medium resolution Survey/ Instrument	$\log N_{\text{HI}}$ cm^{-2}
J004054.7-091526	4.538	20.20 ± 0.09	SDSS	20.22 ± 0.26^1
...	4.740	20.39 ± 0.11	SDSS	20.55 ± 0.15^2
QSO B1114-0822	4.258	20.02 ± 0.12	WHT	20.3^3
J115538.6+053050	2.608	20.37 ± 0.11	SDSS	20.47 ± 0.23^1
...	3.327	21.00 ± 0.10	SDSS	20.91 ± 0.27^1
LBQS 2132-4321	1.916	20.74 ± 0.09	LBQS	20.70^3
J235702.5-004824	2.479	20.41 ± 0.08	SDSS	20.45^2

References: (1) Noterdaeme et al. (2009); (2) Prochaska et al. (2008); (3) Storrie-Lombardi & Wolfe (2000)

the redshift of the sub-DLA. Fig. 2 shows our best fit result of the H α lines.

2. QSO J0008-2901 ($z_{\text{em}} = 2.607$). The quasar was also discovered during the course of the 2dF quasar redshift survey (Croom et al. 2001). An H α absorber at $z = 2.491$ is reported by Tytler et al. (2009). We find that the absorber at $z_{\text{abs}} = 2.491$ is a sub-DLA with $\log N_{\text{HI}} = 19.94 \pm 0.11$ and $b = 39 \pm 3.5 \text{ km s}^{-1}$ detected down to Ly γ . Metal lines from O i λ 1302, Fe ii $\lambda\lambda\lambda\lambda$ 2344, 2374, 2382, 2586, Si ii $\lambda\lambda\lambda\lambda$ 1260, 1304, 1808, C ii λ 1334, Al ii λ 1670, and Si iv $\lambda\lambda$ 1393, 1402 are detected in the red part of the spectrum. Fig. 3 shows our best fit result of the H α lines.
3. QSO J0041-4936 ($z_{\text{em}} = 3.240$). A damped absorber is known in this quasar from the Calán Tololo survey (Maza et al. 1995). From a low-resolution spectrum, Lopez et al. (2001) measured the equivalent width of the H α absorption line to be $\text{EW}_{\text{obs}} = 34.60 \text{ Å}$ but state that they cannot measure the H α column density due to the limited spectral resolution. Using the high-resolution UVES spectrum, we are able to measure the column density of the DLA to be $\log N_{\text{HI}} = 20.46 \pm 0.13$ and $b = 29 \pm 3.9 \text{ km s}^{-1}$ at $z_{\text{abs}} = 2.248$ detected down to Ly β . Metal lines from O i

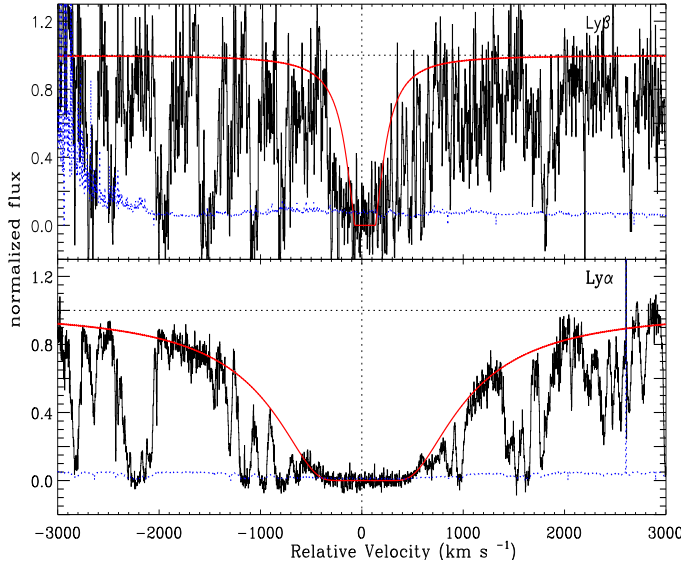


Fig. 4. The DLA detected towards QSO J0041-4936 at $z_{abs} = 2.248$. For plotting purposes the Ly β region of the spectrum is smoothed with a boxcar average of 2.0 pixels. The solid red line represents the Voigt profile fit to the DLA with an inferred column density of $\log N_{HI} = 20.46 \pm 0.13$. The system is detected down to Ly β .

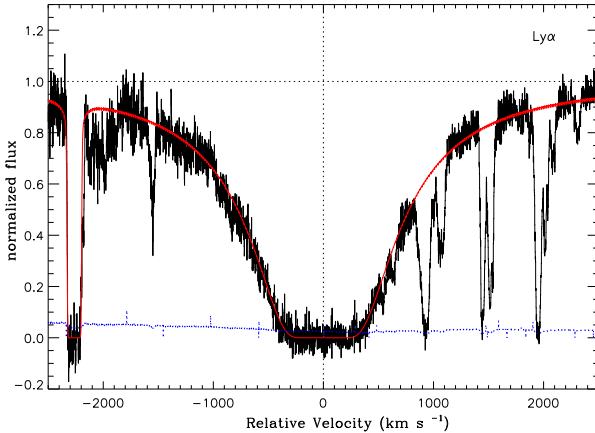


Fig. 5. The sub-DLA detected towards QSO B0128-2150 at $z_{abs} = 1.857$. The solid red line shows the Voigt profile fit to the sub-DLA with an inferred column density of $\log N_{HI} = 20.21 \pm 0.09$.

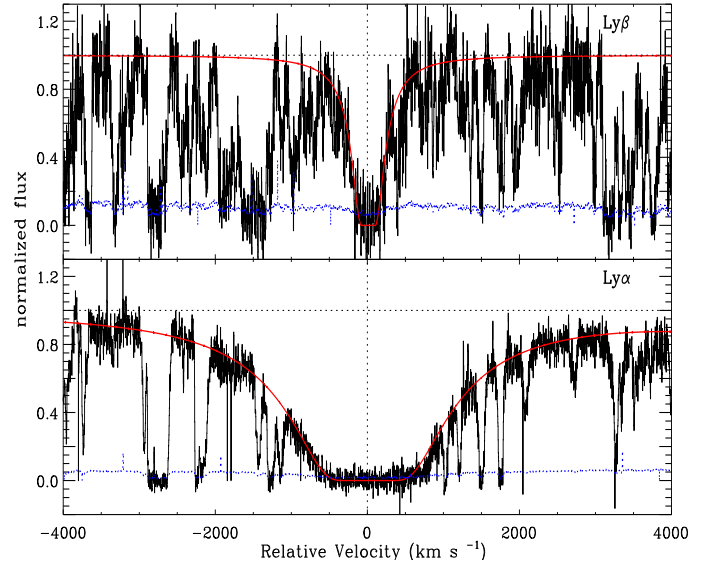


Fig. 6. The DLA detected towards J021741.8-370100 at $z_{abs} = 2.429$. The solid red line represents the Voigt profile fit to the DLA with an inferred column density of $\log N_{HI} = 20.62 \pm 0.08$. The system is detected down to Ly β .

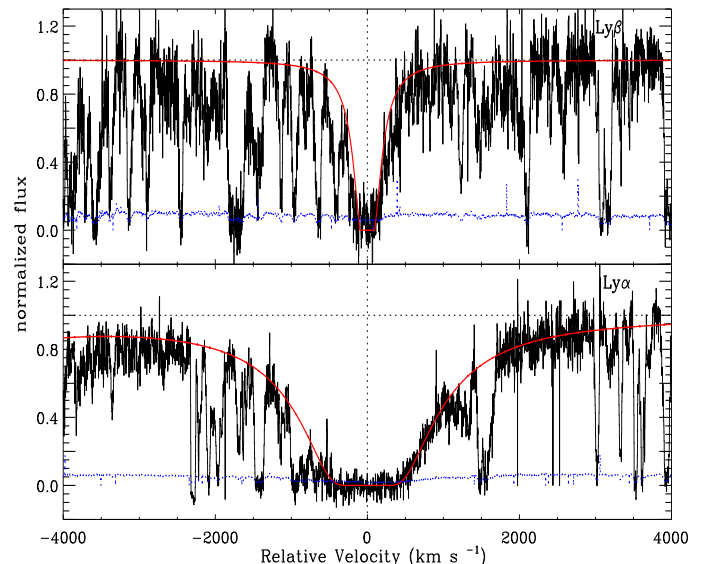


Fig. 7. The DLA detected towards J021741.8-370100 at $z_{abs} = 2.514$. The solid red line corresponds to the Voigt profile fit to the DLA with an inferred column density of $\log N_{HI} = 20.46 \pm 0.13$. The system is detected down to Ly β .

$\lambda 1302$, Fe II $\lambda\lambda 1608, 1611$, Si II $\lambda\lambda\lambda 1260, 1304, 1526, 1808$, C II $\lambda 1334$, Al II $\lambda 1670$, Zn II $\lambda 2026$, Al III $\lambda\lambda 1854, 1862$, and C IV $\lambda\lambda 1548, 1550$ associated with the DLA are detected in the red part of the spectrum. Fig. 4 shows the best fit result of the H I lines.

4. QSO B0128-2150 ($z_{em} = 1.900$). This quasar was discovered during the course of the Montréal-Cambridge-Tololo survey (Lamontagne et al. 2000). Two absorbing systems at $z_{abs} = 1.64$ and 1.85 are reported in the UVES observing proposal. We find that the system at $z_{abs} = 1.857$ is a sub-DLA with $\log N_{HI} = 20.21 \pm 0.09$ and $b = 25 \pm 2.6 \text{ km s}^{-1}$. Metal lines from O I $\lambda 1302$, Fe II $\lambda\lambda\lambda 2344, 2374, 2382$, Si II $\lambda\lambda\lambda 1260, 1304, 1808$, C II $\lambda 1334$, and Al III $\lambda\lambda 1854, 1862$ at the redshift of the absorber are observed in the red part of the spectrum.

Fig. 5 shows our best fit result of the H I column density. The absorbing system at $z_{abs} = 1.64$ is below sub-DLA limit.

5. J021741.8-370100 ($z_{em} = 2.910$). Damped absorbers have been known in this quasar from the Calán Tololo survey (Maza et al. 1996). The column densities for these DLAs have not been reported before. We measure $\log N_{HI} = 20.62 \pm 0.08$ at $z_{abs} = 2.429$ and $\log N_{HI} = 20.46 \pm 0.09$ at $z_{abs} = 2.514$. Both absorbers are seen down to Ly β . The b parameter is fixed to $b = 30 \text{ km s}^{-1}$ for both absorbers. Due to limited wavelength coverage only a few metal lines associated with the absorbers are seen in the spectrum. Metal lines from O I $\lambda 1302$ and Si II $\lambda\lambda\lambda 1190, 1193, 1260, 1304$ are covered for the absorber at $z_{abs} = 2.429$. The lines from

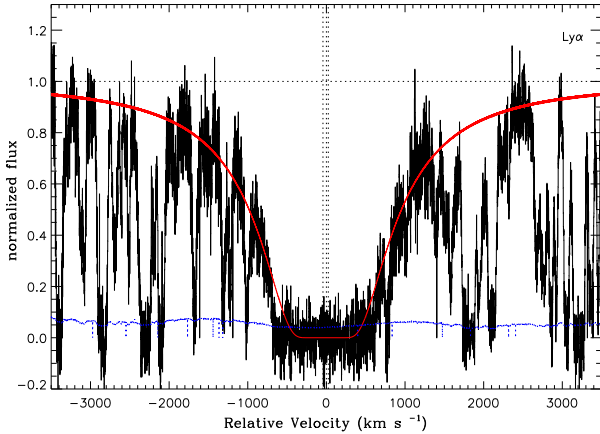


Fig. 8. The DLA detected towards J060008.1-504036 at $z_{\text{abs}} = 2.149$. The solid red line shows the Voigt profile fit to the DLA with a total column density of $\log N_{HI} = 20.40 \pm 0.12$ using velocity components at 24, 0, -44 km s^{-1} .

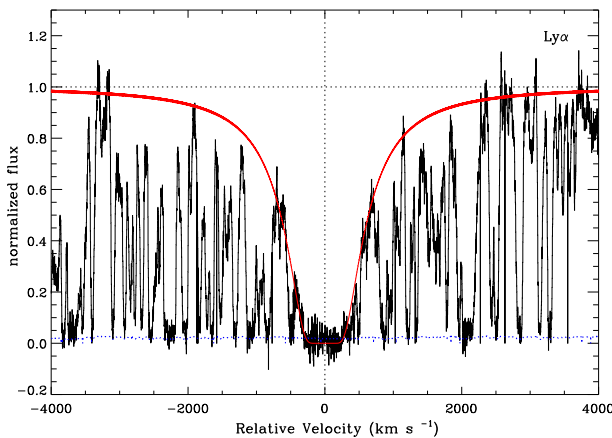


Fig. 9. The sub-DLA detected towards J0952-0115 at $z_{\text{abs}} = 3.476$. The solid red line corresponds to the Voigt profile fit to the sub-DLA with an inferred column density of $\log N_{HI} = 20.04 \pm 0.07$.

- Fe II $\lambda 1144$ and Si II $\lambda\lambda\lambda 1190, 1193, 1260$ associated with the absorber at $z_{\text{abs}} = 2.514$ are covered in the spectrum. Fig. 6 and Fig. 7 show our best fit of H I lines for absorbers at $z_{\text{abs}} = 2.429$ and $z_{\text{abs}} = 2.514$ respectively.
6. J060008.1-504036 ($z_{\text{em}} = 3.130$). This quasar was discovered during the course of the Calán Tololo survey (Maza et al. 1996). No detailed analysis of this quasar has been published. A Lyman limit system at $z_{\text{LLS}} = 3.080$ is seen in the spectrum. We identified a DLA at $z_{\text{abs}} = 2.149$. The column density of the DLA is fitted using three strong components (at 24, 0, and -44 km s^{-1}) seen in O I, resulting in a total column density of $\log N_{HI} = 20.40 \pm 0.12$ with $b = 20 \text{ km s}^{-1}$ fixed for each component. Metal absorption lines from O I $\lambda 1302$, Fe II $\lambda\lambda 1608, 1611$, Si II $\lambda\lambda\lambda 1260, 1304, 1526$, Al II $\lambda 1670$, Al III $\lambda\lambda 1854, 1862$, and C IV $\lambda\lambda 1548, 1550$ associated with the sub-DLA are covered in the red part of the spectrum. Fig. 8 shows our best fit of the neutral hydrogen column density of the DLA at $z_{\text{abs}} = 2.149$.
 7. QSO B0952-0115 ($z_{\text{em}} = 4.426$). One damped absorber was previously reported in this quasar at $z_{\text{abs}} = 4.024$ (Storrie-Lombardi & Wolfe 2000; Prochaska et al. 2007). A Lyman limit system at $z_{\text{LLS}} = 4.242$ is detected in the spec-

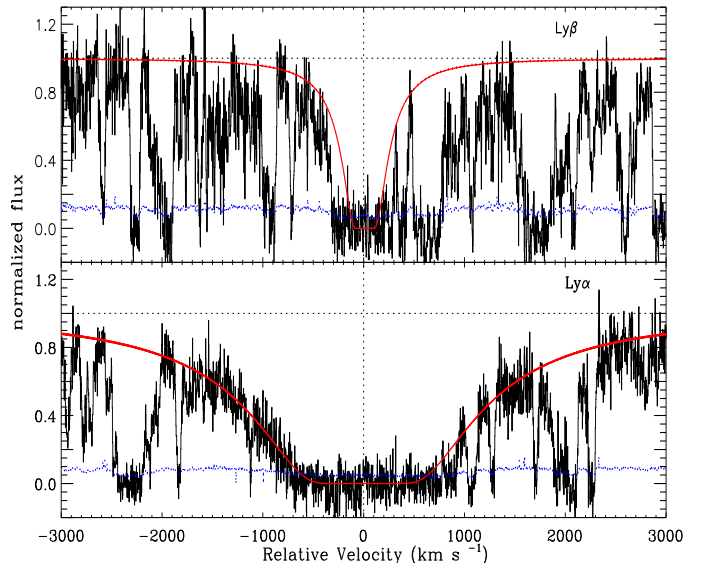


Fig. 10. The DLA detected towards QSO 1036-272 at $z_{\text{abs}} = 2.792$. The solid red line represents the Voigt profile fit to the DLA with an inferred column density of $\log N_{HI} = 20.65 \pm 0.13$. The system is detected down to Lyβ.

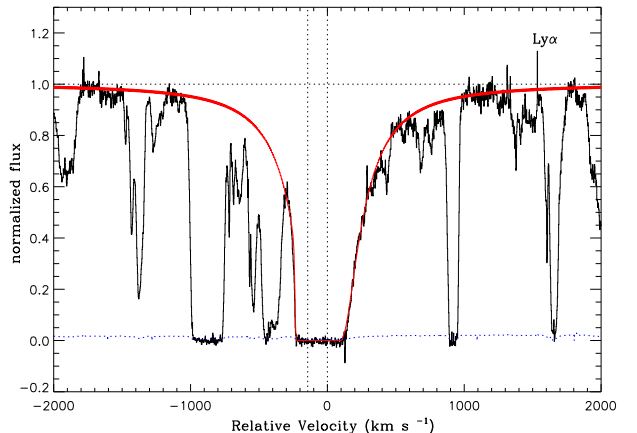


Fig. 11. The sub-DLA detected towards QSO 1036-2257 at $z_{\text{abs}} = 2.533$. The solid red line represents the Voigt profile fit to the sub-DLA with a total column density of $\log N_{HI} = 19.30 \pm 0.10$ fitted with two velocity components at 0 and -144 km s^{-1} .

trum. We find a sub-DLA at $z_{\text{abs}} = 3.476$ with $\log N_{HI} = 20.04 \pm 0.07$ and $b = 32 \pm 3.9 \text{ km s}^{-1}$. Metal lines from Fe II $\lambda\lambda 1608, 1611$, Si II $\lambda\lambda\lambda 1260, 1304, 1526$, Al II $\lambda 1670$, Al III $\lambda\lambda 1854, 1862$, and C IV $\lambda\lambda 1548, 1550$ associated with the sub-DLA are covered in the red part of the spectrum. Fig. 9 shows the best fit result of the H I column density.

8. Q1036-272 ($z_{\text{em}} = 3.090$). A low-resolution spectrum of this quasar has been previously published (Jakobsen & Perryman 1992). We report a DLA with H I column density of $\log N_{HI} = 20.65 \pm 0.13$ and $b = 35 \pm 5 \text{ km s}^{-1}$ down to Lyβ at $z_{\text{abs}} = 2.792$. Several metal absorption lines from O I $\lambda 1302$, Fe II $\lambda\lambda\lambda 1144, 2344, 2374, 2382$, Si II $\lambda\lambda\lambda 1190, 1193, 1260, 1304$, and Al III $\lambda\lambda 1854, 1862$ are covered in the red part of the spectrum. Fig. 10 shows best fit result of the H I lines at $z_{\text{abs}} = 2.792$.

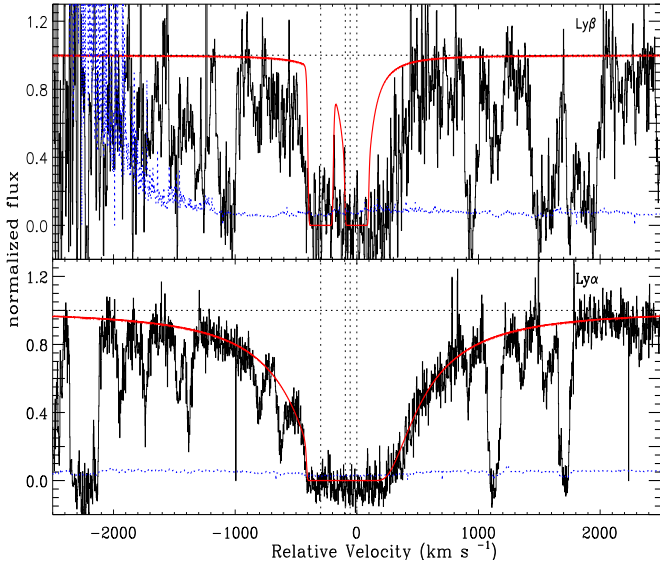


Fig. 12. The sub-DLA detected towards QSO B1036-268 at $z_{\text{abs}} = 2.235$. Ly β region of the spectrum is smoothed with a boxcar average of 2.0 pixels for plotting purposes. The solid red line corresponds to the Voigt profile fit to the sub-DLA with a total column density of $\log N_{HI} = 19.96 \pm 0.09$ from 0, -55, -95, and -297 km s^{-1} velocity components. The system is detected down to Ly β .

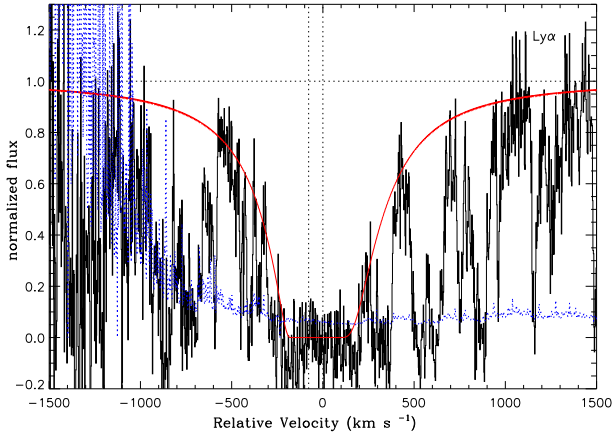


Fig. 13. The sub-DLA detected towards LBQS 1232+0815 at $z_{\text{abs}} = 1.720$. The spectrum is smoothed with a boxcar average of 0.5 pixel for plotting purposes. The solid red line represents the Voigt profile fit to the sub-DLA with a total column density of $\log N_{HI} = 19.48 \pm 0.13$ using 0 and -78 km s^{-1} velocity components (see Fig. 14).

9. QSO B1036-2257 ($z_{\text{em}} = 3.130$). A damped and sub-damped absorber were previously reported in this quasar at $z_{\text{abs}} = 2.777$ (Fox et al. 2009) and $z_{\text{abs}} = 2.531$ (Lopez et al. 2001) respectively. A Lyman limit system at $z_{\text{LLS}} = 2.792$ is also detected. From a low-resolution spectrum, Lopez et al. (2001) measured the equivalent width of the H I absorption line to be $EW_{\text{obs}} = 13.52 \text{ \AA}$ but state that they cannot measure the H I column density due to the limited spectral resolution. Using the high-resolution UVES spectrum, we are able to identify two main components in the system from the metal lines at 0 and -144 km s^{-1} . Fitting these components we measure the total column density of the sub-DLA to be

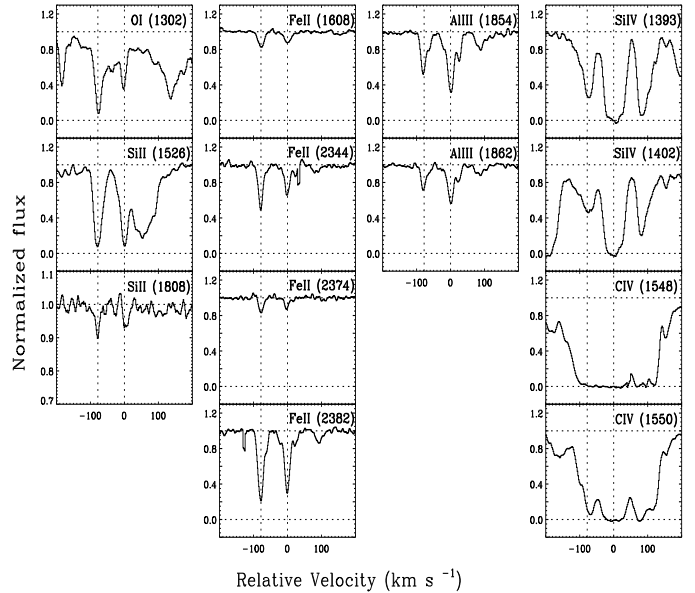


Fig. 14. Low and high ionization metal lines associated with the sub-DLA at $z_{\text{abs}} = 1.720$ (zero velocity) along the line-of-sight of LBQS 1232+0815 are shown. The line IDs are given in each panel.

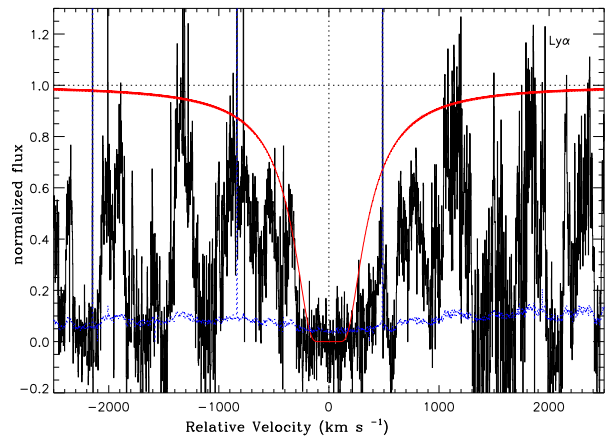


Fig. 15. The sub-DLA detected towards QSO J1330-2522 at $z_{\text{abs}} = 2.654$. The solid red line shows the Voigt profile fit to the sub-DLA with an inferred column density of $\log N_{HI} = 19.56 \pm 0.13$.

- log $N_{HI} = 19.30 \pm 0.10$ with b parameter of $b = 26 \pm 3.4$ and fixed 20 km s^{-1} (at 0 and -144 km s^{-1}). The component at 0 km s^{-1} is stronger and heavily dominates over the component at 144 km s^{-1} . Metal lines from Fe II $\lambda\lambda\lambda 1144, 2344, 2382, 2586$, Si II $\lambda\lambda\lambda 1193, 1260, 1526$, C II $\lambda 1334$, Al III $\lambda\lambda 1854, 1862$, Si IV $\lambda\lambda 1393, 1402$, and C IV $\lambda\lambda 1548, 1550$ associated with the sub-DLA are detected in the red part of the spectrum. Fig. 11 shows the best fit result of the H I column density.
10. QSO B1036-268 ($z_{\text{em}} = 2.460$). A low-resolution slit spectrum of the quasar has been previously published (Jakobsen & Perryman 1992). We find four strong velocity components in the system at $z_{\text{abs}} = 2.235$ from the metal lines. The column density of the sub-DLA fitted down to Ly β with four components at 0, -55, -95, and -144 km s^{-1} , resulting a total of $\log N_{HI} = 19.96 \pm 0.09$ and $b = 20, 20, 20$

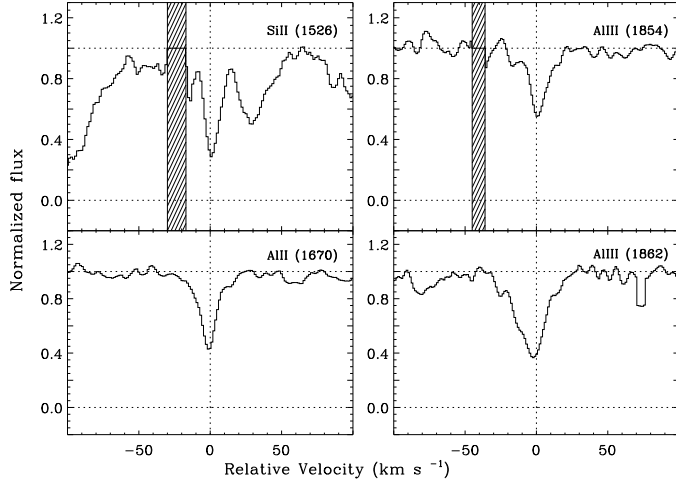


Fig. 16. Low ionization metal lines associated with the sub-DLA at $z_{abs} = 2.654$ along the line-of-sight of LBQS 1330-2522. The vertical dashed line is adopted zero velocity corresponding to $z_{abs} = 2.654$. The line IDs are given in each panel. The shaded area corresponds to the regions affected by cosmic rays.

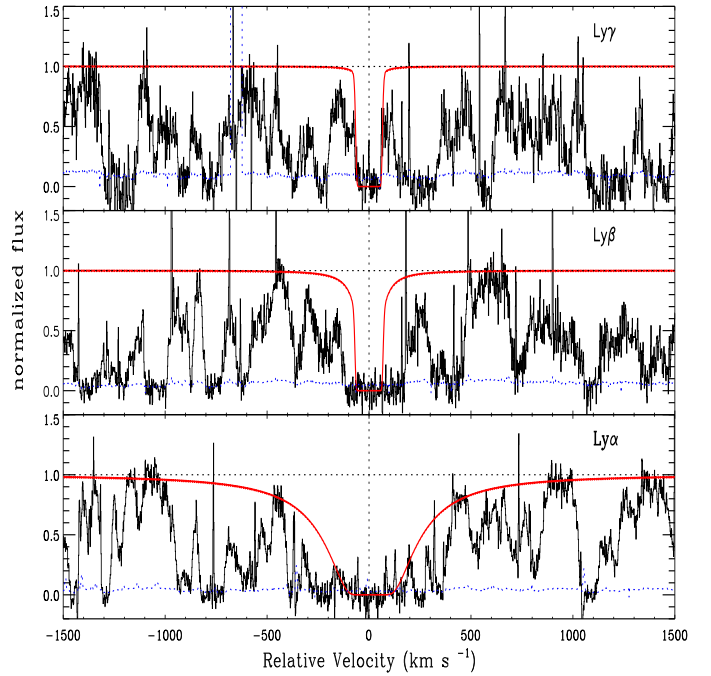


Fig. 18. The sub-DLA detected towards J1723+2243 at $z_{abs} = 4.155$. The solid red line corresponds to the Voigt profile fit to the sub-DLA with an inferred column density of $\log N_{HI} = 19.23 \pm 0.12$. The system is detected down to the Ly γ range.

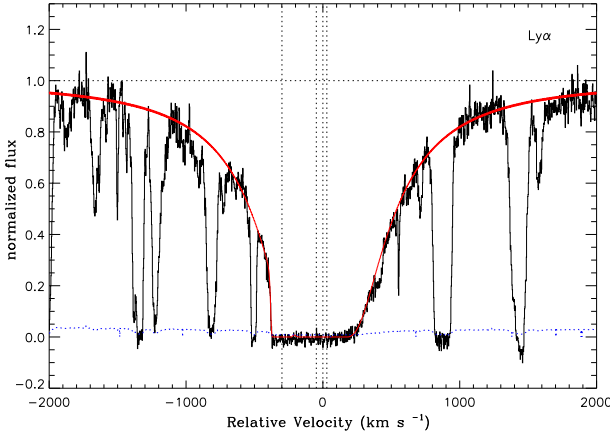


Fig. 17. The sub-DLA detected towards QSO J1356-1101 at $z_{abs} = 2.397$. The solid red line represents the Voigt profile fit to the sub-DLA with a total column density of $\log N_{HI} = 19.88 \pm 0.09$ using 29, 0, -48 and -300 km s^{-1} velocity components.

(fixed), and $35 \pm 3.0 \text{ km s}^{-1}$ respectively. The component at 0 km s^{-1} is strongest and heavily dominates over other components. Strong metal absorption lines from O I $\lambda 1302$, Fe II $\lambda\lambda\lambda\lambda\lambda\lambda 1144, 1608, 1611, 2344, 2374, 2382, 2586$, Si II $\lambda\lambda\lambda\lambda 1190, 1193, 1260, 1304, 1526$, C II $\lambda 1334$, Al II $\lambda 1670$, Mg II $\lambda\lambda 2796, 2803$, Al III $\lambda\lambda 1854, 1862$, Si IV $\lambda\lambda 1393, 1402$, and C IV $\lambda\lambda 1548, 1550$ at the redshift of the sub-DLA are covered in the red part of the spectrum. Fig. 12 shows our best fit result of H I lines of the sub-DLA.

11. LBQS 1232+0815 ($z_{em} = 2.570$). A DLA was known at $z_{abs} = 2.338$ along the line-of-sight of this quasar (Prochaska et al. 2007; Ivanchik et al. 2010). We report for the first time a sub-DLA at $z_{abs} = 1.720$ with total $\log N_{HI} = 19.48 \pm 0.13$. From O I, we identified two main velocity components from the system at 0 and -78 km s^{-1} (see Fig. 14) where b is fixed at $b = 20 \text{ km s}^{-1}$ for both components. Metal absorption lines from O I $\lambda 1302$, Fe II $\lambda\lambda\lambda\lambda\lambda\lambda 1608, 1611, 2344, 2374, 2382$, Si II $\lambda\lambda 1526, 1808$, Al III $\lambda\lambda 1854, 1862$, Si IV $\lambda\lambda 1393, 1402$, and C IV $\lambda\lambda 1548, 1550$ associated with the sub-DLA are covered in the red part of the spectrum. Fig. 13 shows the best fit result of H I column density of the sub-DLA. While the Ly α line is noisy, the presence of the sub-DLA is confirmed through the metal lines detected in the spectrum (see Fig. 14).

12. QSO J1330-2522 ($z_{em} = 3.910$). Two sub-DLAs were previously reported at $z_{abs} = 2.910$ and 3.080 (Péroux et al. 2001) along the line-of-sight of this quasar. A Lyman limit system at $z_{LLS} = 3.728$ is also seen. We report a new sub-DLA at $z_{abs} = 2.654$ with neutral hydrogen column density of $\log N_{HI} = 19.56 \pm 0.13$ and $b = 25.5 \pm 2.4 \text{ km s}^{-1}$. Fig. 15

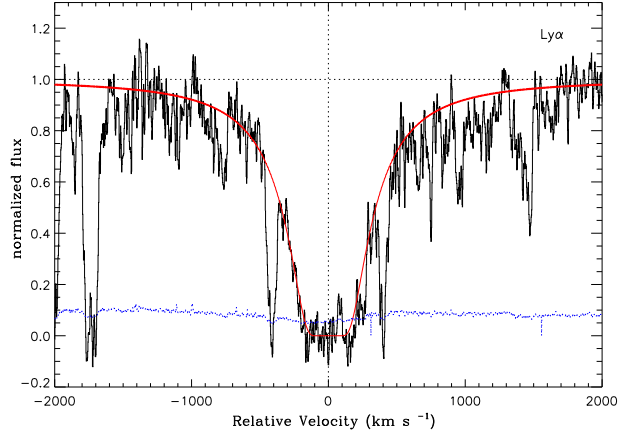


Fig. 19. The sub-DLA detected towards LBQS 2114-4347 at $z_{abs} = 1.912$. For plotting purposes the spectrum is smoothed with a boxcar average of 1.0 pixel. The solid red line shows the Voigt profile fit to the sub-DLA with an inferred column density of $\log N_{HI} = 19.50 \pm 0.10$.

1862, Si IV $\lambda\lambda 1393, 1402$, and C IV $\lambda\lambda 1548, 1550$ associated with the sub-DLA are covered in the red part of the spectrum. Fig. 13 shows the best fit result of H I column density of the sub-DLA. While the Ly α line is noisy, the presence of the sub-DLA is confirmed through the metal lines detected in the spectrum (see Fig. 14).

12. QSO J1330-2522 ($z_{em} = 3.910$). Two sub-DLAs were previously reported at $z_{abs} = 2.910$ and 3.080 (Péroux et al. 2001) along the line-of-sight of this quasar. A Lyman limit system at $z_{LLS} = 3.728$ is also seen. We report a new sub-DLA at $z_{abs} = 2.654$ with neutral hydrogen column density of $\log N_{HI} = 19.56 \pm 0.13$ and $b = 25.5 \pm 2.4 \text{ km s}^{-1}$. Fig. 15

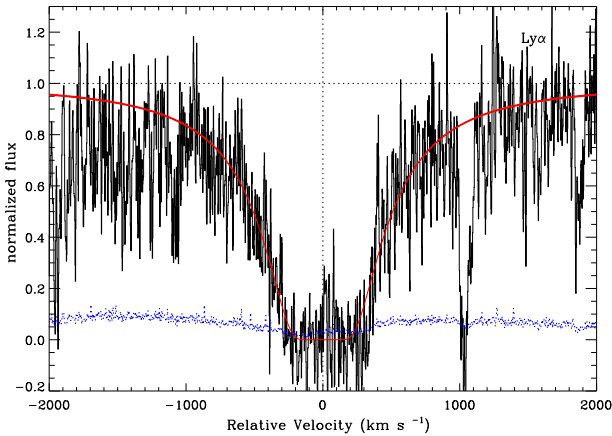


Fig. 20. The sub-DLA detected towards J223941.8-294955 at $z_{\text{abs}} = 1.825$. The spectrum is smoothed with a boxcar average of 1.0 pixel for plotting reasons. The solid red line corresponds to the Voigt profile fit to the sub-DLA with an inferred column density of $\log N_{\text{HI}} = 19.84 \pm 0.14$. Emission is clearly seen in the trough of this absorber which is likely to correspond to the Lyman- α emission from the sub-DLA host.

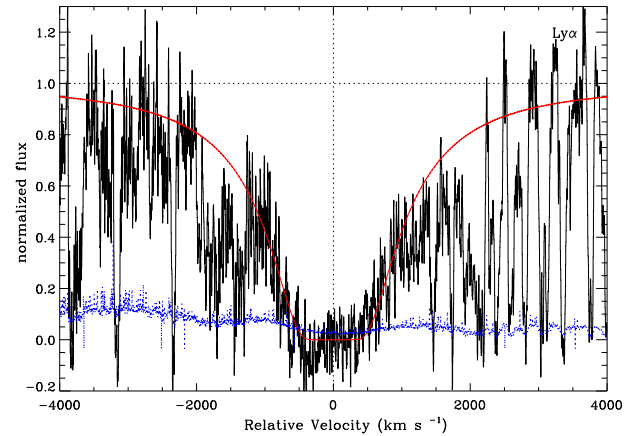


Fig. 21. The DLA detected towards QSO B2318-1107 at $z_{\text{abs}} = 1.629$. For plotting purposes the spectrum is smoothed with a boxcar average of 0.5 pixel. The solid red line corresponds to the Voigt profile fit to the DLA with an inferred column density of $\log N_{\text{HI}} = 20.52 \pm 0.14$.

shows our best fit result. Metal lines from Si II $\lambda\lambda\lambda 1260, 1526, 1808$, Al II $\lambda 1670$, Al III $\lambda\lambda 1854, 1862$, Si IV $\lambda\lambda 1393, 1402$, and C IV $\lambda\lambda 1548, 1550$ are covered in the red part of the spectrum at the redshift of the sub-DLA. As an example of metal lines, low ionization lines from the sub-DLA confirming its presence are plotted in Fig. 16. High ionization lines are blended with the lines from the other two sub-DLAs.

13. QSO J1356-1101 ($z_{\text{em}} = 3.006$). Two damped absorbers have been previously reported in this quasar at $z_{\text{abs}} = 2.501$ and 2.967 (Prochaska et al. 2007; Noterdaeme et al. 2008; Fox et al. 2009). We report for the first time a sub-DLA at $z_{\text{abs}} = 2.397$ in the quasar. From the O I, we find four strong components in the system at 29, 0, -48, and -300 km s $^{-1}$. The total H I column density of the system is $\log N_{\text{HI}} = 19.88 \pm 0.09$ with $b = 20, 20, 20$, (fixed) 28 ± 2.8 km s $^{-1}$ for 29, 0, -48, and -300 km s $^{-1}$ components respectively. The component at 0 km s $^{-1}$ is strongest and heavily dominates over other components. Metal absorption lines from O I $\lambda 1302$, Fe II $\lambda\lambda\lambda\lambda 1144, 2344, 2374, 2382, 2586$, and Si II $\lambda\lambda\lambda 1190, 1193, 1260, 1304$ associated with the sub-DLA are detected in the red part of the spectrum. Fig. 17 shows the best fit result of the neutral hydrogen column density of the sub-DLA.
14. QSO J1723+2243 ($z_{\text{em}} = 4.520$). A damped absorber has been previously reported in this quasar at $z_{\text{abs}} = 3.697$ (Prochaska et al. 2007; Guimarães et al. 2009). We observed a sub-DLA down to Ly γ at $z_{\text{abs}} = 4.155$ with H I column of $\log N_{\text{HI}} = 19.23 \pm 0.12$ with a fixed $b = 20$ km s $^{-1}$. The metal lines associated with this system are either blended with other features or not covered by our data so that this detection is based on the Lyman line only and is a little less secure than the others. The detection of absorption lines from the Lyman series confirm the presence of the sub-DLA. Fig. 18 shows our best fit result of H I lines.
15. LBQS 2114-4347 ($z_{\text{em}} = 2.040$). The quasar has been discovered as part of the Large Bright Quasar Survey (LBQS; Morris et al. 1991). No absorber has been previously reported in this quasar (Péroux et al. 2003b). We observed, for

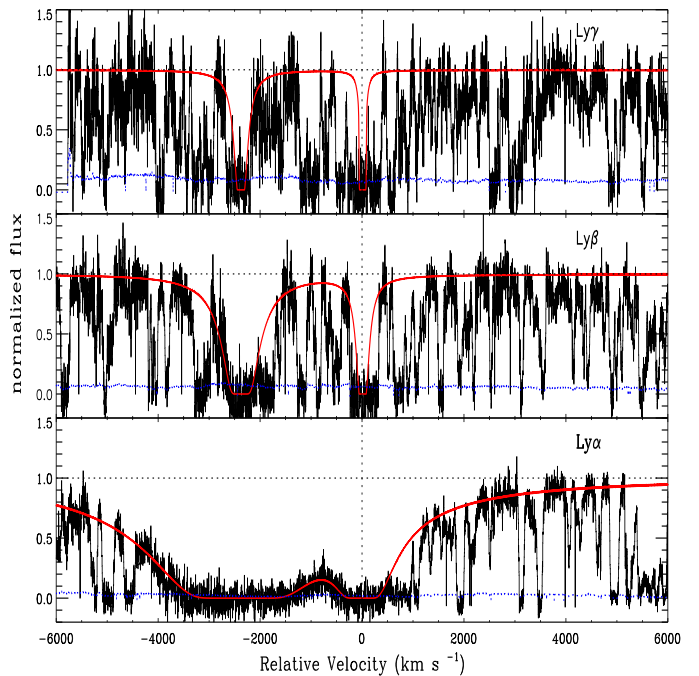


Fig. 22. The sub-DLA detected towards QSO B2342+3417 at $z_{\text{abs}} = 2.940$. The solid red line corresponds to the Voigt profile fit to the sub-DLA with an inferred column density of $\log N_{\text{HI}} = 20.18 \pm 0.10$. The system is fitted simultaneously with a high column density absorber at $z_{\text{abs}} = 2.909$ ($\log N_{\text{HI}} = 21.10 \pm 0.10$) to determine the column density precisely.

the first time, a sub-DLA at $z_{\text{abs}} = 1.912$ with best fit column density of $\log N_{\text{HI}} = 19.50 \pm 0.10$ and $b = 31.7 \pm 3.4$ km s $^{-1}$. Several metal absorption lines from O I $\lambda 1302$, Fe II $\lambda\lambda\lambda\lambda 1144, 1608, 2344, 2374, 2382, 2586$, Si II $\lambda\lambda\lambda\lambda 1193, 1260, 1304, 1526, 1808$, C II $\lambda 1334$, Al II $\lambda 1670$, Mg II $\lambda\lambda 2796, 2803$, Si IV $\lambda\lambda 1393, 1402$, and C IV $\lambda\lambda 1548, 1550$ at the redshift of the sub-DLA are covered in the red part of the spectrum. Fig. 19 shows our best fit of H I column density.

16. J223941.8-294955 ($z_{em} = 2.102$). This quasar was discovered during the course of the 2dF quasar redshift survey. The absorber at $z_{abs} = 1.825$ in this quasar has been reported before by Cappetta et al. (2010) with a column density of $\log N_{HI} = 20.60$ (where H α fit was not shown). We fit the H α of the absorber again and find that the absorber at $z_{abs} = 1.825$ fits well with H α column density of $\log N_{HI} = 19.84 \pm 0.14$ and $b = 53.0 \pm 4.7 \text{ km s}^{-1}$. Emission is clearly seen in the trough of this absorber which is likely to correspond to the Lyman- α emission from the sub-DLA host. Several metal absorption lines from O I $\lambda 1302$, Fe II $\lambda\lambda\lambda\lambda\lambda\lambda 1144, 1608, 2344, 2374, 2382, 2586$, Si II $\lambda\lambda\lambda\lambda\lambda\lambda 1193, 1260, 1304, 1526, 1808$, C II $\lambda 1334$, Al II $\lambda 1670$, Mg II $\lambda\lambda 2796, 2803$, Al III $\lambda\lambda 1854, 1862$, Si IV $\lambda\lambda 1393, 1402$, and C IV $\lambda\lambda 1548, 1550$ associated with sub-DLA are covered in the red part of the spectrum. Fig. 20 shows our best fit result of neutral hydrogen column density fit.
17. QSO B2318-1107 ($z_{em} = 2.960$). A DLA was previously known at $z_{abs} = 1.989$ along the line-of-sight of the quasar (Noterdaeme et al. 2007; Fox et al. 2009). We find a new DLA in the quasar at $z_{abs} = 1.629$ with neutral hydrogen column of $\log N_{HI} = 20.52 \pm 0.14$ with fixed $b = 30.0 \text{ km s}^{-1}$. Several metal absorption lines from Fe II $\lambda\lambda\lambda\lambda\lambda\lambda 1608, 1611, 2344, 2374, 2382$, Si II $\lambda\lambda\lambda\lambda\lambda\lambda 1193, 1260, 1304, 1526$, C II $\lambda 1334$, Al II $\lambda 1670$, Al III $\lambda\lambda 1854, 1862$, and Si IV $\lambda\lambda 1393, 1402$ associated with the DLA are covered in the red part of the spectrum. Fig. 21 shows our best fit of the H α column to the DLA.
18. QSO B2342+3417 ($z_{em} = 3.010$). A damped absorber with $\log N_{HI} = 21.10 \pm 0.10$ was previously reported at $z_{abs} = 2.909$ in the quasar (Prochaska et al. 2003; Fox et al. 2009). A joint fit was implemented by Prochaska et al. (2003) to fit the DLA together with the neighboring sub-DLA, but the column density of the sub-DLA was not reported. We measure $\log N_{HI} = 20.18 \pm 0.10$ down to Ly γ at $z_{abs} = 2.940$ with a fixed $b = 20.0 \text{ km s}^{-1}$. The metal lines associated with this system are not seen because of limited wavelength coverage in the red part of the spectrum. Fig. 22 shows the best fit result of the H α lines.

3.3. DLAs/sub-DLAs towards EUADP quasars

Besides the 150 DLAs/sub-DLAs, we found another 47 damped absorbers (21 DLAs and 26 sub-DLAs) in the literature along the lines-of-sight of our 250 EUADP quasars, for which Ly α absorption lines are not covered by our data either due to the limited wavelength coverage or non-overlapping settings. These systems are however of interest to us because their metal lines might still be included in our data and are helpful in further studies of the EUADP sample. These 150 and 47 damped absorbers (with and without Ly α covered by the EUADP dataset) make up a total of 197 DLAs/sub-DLAs along lines-of-sight of the 250 EUADP quasars where 114 are DLAs and 83 are sub-DLAs. The EUADP sample by design is biased towards DLAs and therefore we see less sub-DLAs than DLAs in the sample. Indeed, in the redshift range $0.2 < z < 4.9$, we expect twice as many sub-DLAs as DLAs based on the number density of absorbers at a mean redshift of $z = 2.4$ (see Péroux et al. 2005).

4. Global Properties of the EUADP sample

The emission redshifts of the 250 EUADP sample quasars are initially obtained from the Simbad catalogue and later double checked for the cases where Ly α emission from the

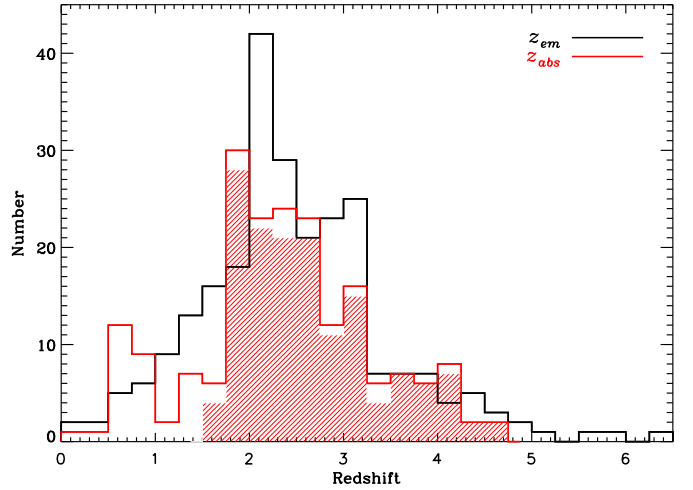


Fig. 23. Distribution of quasar emission redshift of the EUADP sample (black histogram). The red histogram shows the redshift distribution of DLAs/sub-DLAs along the lines-of-sight of EUADP quasars. The red shaded area corresponds to the distribution of the 150 damped absorbers with Ly α covered by our EUADP sample.

quasar is covered by our data. The Ly α emission for 5 quasars (i.e., QSO J0332-4455, QSO B0528-2505, QSO B0841+129, QSO B1114-0822 and QSO J2346+1247) is not seen because of the presence of DLAs belonging to the “proximate DLA” class with $z_{abs} \approx z_{em}$ (e.g., Møller et al. 1998; Ellison et al. 2011; Zafar et al. 2011). For the emission redshifts of these 5 cases, we rely on the literature. The emission redshifts of all the other objects in the EUADP sample have been compared with measurements from the literature. For a few cases, emission redshifts provided in the Simbad catalogue are not correct and the correct redshifts are obtained from the literature. In our sample, there are 38 quasars with emission redshifts below $z_{em} < 1.5$. For these cases we cannot see Ly α emission from the quasar because of the limited spectral coverage, therefore, we relied mostly on the Simbad catalogue. However, other emission lines are covered in the spectra, helping us to confirm the emission redshifts. The emission redshifts of 250 quasars of EUADP sample ranges from $0.191 \leq z_{em} \leq 6.311$. Their distribution is shown in Fig. 23 and is found to peak at $z_{em} \approx 2.1$.

In Fig. 24, the column density distribution of DLAs and sub-DLAs is presented (see Zafar et al. 2013 for complete list of DLAs and sub-DLAs H α column densities). It is worth noting that in the EUADP sample, damped absorbers with column densities up to $\log N_{HI} = 21.85$ are seen, while higher column densities have been recently reported (Guimarães et al. 2012; Kulkarni et al. 2012; Noterdaeme et al. 2012a). As mentioned above in the EUADP sample, the number of sub-DLAs is lower than the number of DLAs. Indeed, a large fraction (~45%) of the quasars in the EUADP sample were observed because of a known strong damped absorber along their line-of-sight. A carefully selected subset of the EUADP will have to be built for the purpose of statistical analysis of DLAs and sub-DLAs (Zafar et al. 2013).

5. Lines-of-sight of Interest

In the EUADP sample, a few lines-of-sight of quasars are rich and contain more than one absorber. One interesting example is the line-of-sight of QSO J0133+0400, containing six

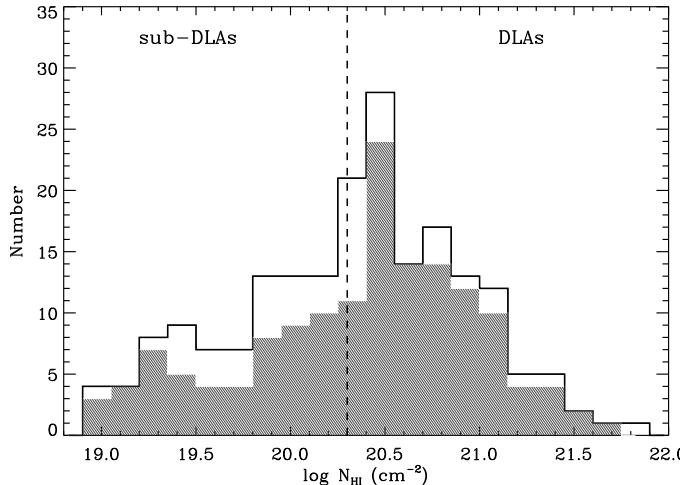


Fig. 24. Histogram showing the number of DLAs and sub-DLAs along lines-of-sight to the quasars in the EUADP sample. The shaded area represents the column density distribution of damped absorbers for which the Ly α line is covered by the EUADP data. The vertical dashed line is the dividing line between the sub-DLAs and DLAs classes.

DLAs and sub-DLAs. In this line-of-sight two sub-DLAs $z_{abs} = 3.995/3.999$ are separated by only $\Delta v = 240 \text{ km s}^{-1}$. Three more examples of rich lines-of-sight are: *i*) QSO J0006-6208 with 3 DLAs and one sub-DLA, *ii*) QSO J0407-4410 with 4 DLAs, where three DLAs have $\log N_{HI} \gtrsim 21.0$, and *iv*) QSO B0841+129 containing 3 DLAs (with $\log N_{HI} \gtrsim 21.0$) and one sub-DLA. Such complex group or systems can be classified as multiple DLAs (MDLAs; Lopez & Ellison 2003).

In addition, there are four quasar pairs in the EUADP sample: *i*) QSO J0008-2900 & QSO J0008-2901 separated by $1.3'$. Two sub-DLAs at $z = 2.254$ and $z = 2.491$ are seen along the lines of sight of QSO J0008-2900 and QSO J0008-2901 respectively. *ii*) J030640.8-301032 & J030643.7-301107 separated by ~ 0.85 arcmin and no absorber is seen along the line-of-sight to the pair. *iii*) QSO B0307-195A & B separated by ~ 1 arcmin. A sub-DLA (at $z = 1.788$ with $\log N_{HI} = 19.00 \pm 0.10$) along the line-of-sight of QSO B0307-195B is detected (D'Odorico et al. 2002), but is not seen in its companion. *iv*) QSO J1039-2719 & QSO B1038-2712 separated by $17.9'$. A sub-DLA (at $z = 2.139$ with $\log N_{HI} = 19.90 \pm 0.05$) along the line-of-sight of QSO J1039-2719 is detected (D'Odorico et al. 2002), but no damped absorber is seen in its companion.

6. Conclusion

In this study, high-resolution spectra taken from the UVES Advanced Data Products archive have been processed and combined to make a sample of 250 individual quasars spectra. The high-resolution spectra of these quasars allow us to detect absorbers down to $\log N_{HI} = 19.00 \text{ cm}^{-2}$. Automated and visual searches for quasar absorbers have been undertaken leading to a sample of 93 DLAs and 57 sub-DLAs. An extensive search in the literature shows that 6 of these DLAs and 13 of these sub-DLAs have their H I column densities measured for the first time, where 10 are new identifications. These new damped absorbers are confirmed by detecting metal lines associated with the absorber and/or lines from the higher members of the Lyman series. The H I column densities of all these new absorbers are determined by fitting a Voigt profile to the Ly α line together with the lines

from higher order of the Lyman series whenever covered. Our data contain five proximate DLA cases and three quasar pairs. We found that a few lines-of-sight of quasars are very rich, particularly the line-of-sight of QSO J0133+0400 which contains six DLAs and sub-DLAs.

In an accompanying paper, (Zafar et al. 2013), we use a carefully selected subset of this dataset to study the statistical properties of DLAs and sub-DLAs, measure their column density distribution, and quantify the contribution of sub-DLAs to the H I gas mass density. Further studies using specifically designed subsets of the EUADP dataset will follow.

7. Acknowledgments

This work has been funded within the BINGO! ('history of Baryons: INtergalactic medium/Galaxies cO-evolution') project by the Agence Nationale de la Recherche (ANR) under the allocation ANR-08-BLAN-0316-01. We would like to thank the ESO staff for making the UVES Advanced Data Products available to the community. We are thankful to Stephan Frank, Jean-Michel Deharveng and Bruno Milliard for helpful comments.

References

- Bouché N., Lehnert M. D., Aguirre A., Péroux C., Bergeron J., 2007, MNRAS, 378, 525
- Bouché N., Lehnert M. D., Péroux C., 2005, MNRAS, 364, 319
- Bouché N., Lehnert M. D., Péroux C., 2006, MNRAS, 367, L16
- Cappetta M., D'Odorico V., Cristiani S., Saitta F., Viel M., 2010, MNRAS, 407, 1290
- Croom S. M., Smith R. J., Boyle B. J., et al., 2001, MNRAS, 322, L29
- Dekker H., D'Odorico S., Kaufer A., Delabre B., Kotzlowski H., 2000, in Society of Photo-Optical Instrumentation Engineers (SPIE) Conference Series, edited by M. Iye & A. F. Moorwood, vol. 4008 of SPIE Conference Series, 534–545
- Dessauges-Zavadsky M., Péroux C., Kim T.-S., D'Odorico S., McMahon R. G., 2003, MNRAS, 345, 447
- D'Odorico V., Petitjean P., Cristiani S., 2002, A&A, 390, 13
- Ellison S. L., Prochaska J. X., Mendel J. T., 2011, MNRAS, 412, 448
- Fontana A., Ballester P., 1995, The Messenger, 80, 37
- Fox A. J., Prochaska J. X., Ledoux C., Petitjean P., Wolfe A. M., Srianand R., 2009, A&A, 503, 731
- Guimaraes R., Noterdaeme P., Petitjean P., et al., 2012, AJ, 143, 147
- Guimaraes R., Petitjean P., de Carvalho R. R., et al., 2009, A&A, 508, 133
- Ivanchik A. V., Petitjean P., Balashov S. A., et al., 2010, MNRAS, 404, 1583
- Jakobsen P., Perryman M. A. C., 1992, ApJ, 392, 432
- Kulkarni V. P., Khare P., Péroux C., York D. G., Lauroesch J. T., Meiring J. D., 2007, ApJ, 661, 88
- Kulkarni V. P., Meiring J., Som D., et al., 2012, ApJ, 749, 176
- Lamontagne R., Demers S., Wesemael F., Fontaine G., Irwin M. J., 2000, AJ, 119, 21
- Lanzetta K. M., Wolfe A. M., Turnshek D. A., 1995, ApJ, 440, 435
- Lanzetta K. M., Wolfe A. M., Turnshek D. A., Lu L., McMahon R. G., Hazard C., 1991, ApJS, 77, 1
- Ledoux C., Petitjean P., Srianand R., 2003, MNRAS, 346, 209
- Lopez S., Ellison S., D'Odorico S., Kim T.-S., 2007, A&A, 469, 61
- Lopez S., Ellison S. L., 2003, A&A, 403, 573
- Lopez S., Maza J., Masegosa J., Marquez I., 2001, A&A, 366, 387
- Maza J., Wischnjewsky M., Antezana R., 1996, RMxAA, 32, 35
- Maza J., Wischnjewsky M., Antezana R., González L. E., 1995, RMxAA, 31, 119
- Meiring J. D., Kulkarni V. P., Lauroesch J. T., et al., 2008, MNRAS, 384, 1015
- Meiring J. D., Lauroesch J. T., Kulkarni V. P., Péroux C., Khare P., York D. G., 2009, MNRAS, 397, 2037
- Möller P., Warren S. J., Fynbo J. U., 1998, A&A, 330, 19
- Morris S. L., Weymann R. J., Anderson S. F., et al., 1991, AJ, 102, 1627
- Morton D. C., 2003, ApJS, 149, 205
- Noterdaeme P., Laursen P., Petitjean P., et al., 2012a, A&A, 540, A63
- Noterdaeme P., Ledoux C., Petitjean P., Le Petit F., Srianand R., Smette A., 2007, A&A, 474, 393
- Noterdaeme P., Ledoux C., Petitjean P., Srianand R., 2008, A&A, 481, 327
- Noterdaeme P., Petitjean P., Carithers W. C., et al., 2012b, A&A, 547, L1

- Noterdaeme P., Petitjean P., Ledoux C., Srianand R., 2009, A&A, 505, 1087
- Pagel B. E. J., 2002, in Chemical Enrichment of Intracluster and Intergalactic Medium, edited by R. Fusco-Femiano, F. Matteucci, vol. 253 of Astronomical Society of the Pacific Conference Series, 489
- Péroux C., Dessauges-Zavadsky M., D'Odorico S., Kim T.-S., McMahon R. G., 2003a, MNRAS, 345, 480
- Péroux C., Dessauges-Zavadsky M., D'Odorico S., Sun Kim T., McMahon R. G., 2005, MNRAS, 363, 479
- Péroux C., McMahon R. G., Storrie-Lombardi L. J., Irwin M. J., 2003b, MNRAS, 346, 1103
- Péroux C., Storrie-Lombardi L. J., McMahon R. G., Irwin M., Hook I. M., 2001, AJ, 121, 1799
- Pettini M., 2004, in Cosmochemistry. The melting pot of the elements, edited by C. Esteban, R. García López, A. Herrero, F. Sánchez, 257–298
- Pettini M., 2006, in The Fabulous Destiny of Galaxies: Bridging Past and Present, edited by V. Le Brun, A. Mazure, S. Arnouts, D. Burgarella, 319
- Pettini M., Ellison S. L., Steidel C. C., Bowen D. V., 1999, ApJ, 510, 576
- Prochaska J. X., Gawiser E., Wolfe A. M., Cooke J., Gelino D., 2003, ApJS, 147, 227
- Prochaska J. X., Hennawi J. F., Herbert-Fort S., 2008, ApJ, 675, 1002
- Prochaska J. X., Herbert-Fort S., Wolfe A. M., 2005, ApJ, 635, 123
- Prochaska J. X., Wolfe A. M., Howk J. C., Gawiser E., Burles S. M., Cooke J., 2007, ApJS, 171, 29
- Storrie-Lombardi L. J., Wolfe A. M., 2000, ApJ, 543, 552
- Tytler D., Gleed M., Melis C., et al., 2009, MNRAS, 392, 1539
- Wolfe A. M., Gawiser E., Prochaska J. X., 2005, ARA&A, 43, 861
- Wolfe A. M., Lanzetta K. M., Foltz C. B., Chaffee F. H., 1995, ApJ, 454, 698
- Wolfe A. M., Prochaska J. X., Gawiser E., 2003, ApJ, 593, 215
- Zafar T., Møller P., Ledoux C., et al., 2011, A&A, 532, A51
- Zafar T., Péroux C., Popping A., Milliard B., Deharveng J.-M., Frank S., 2013, A&A, 556, A141

